Bi-static Visible Light Backscatter Modelling and Tag Localisation

Yirui Deng, Deepak Mishra and Aruna Seneviratne
School of Electrical Engineering and Telecommunications
University of New South Wales
Sydney, Australia
Emails: yirui.deng@student.unsw.edu.au, d.mishra@unsw.edu.au and a.seneviratne@unsw.edu.au

***Abstract*—Backscattering visible light communication (VLC) is an emerging technology in the field of indoor communication and the internet-of-things. Here, bi-static topology has gained recent interest in radio-frequency (RF) backscatter communication systems due its longer range and higher scalability. However, the difference between VLC and RF systems raises the demand for new bi-static VLC backscatter models to accurately describe the characteristics. In this paper, we present two novel models designed with specular and diffuse reflectors respectively. We also present the global optimal tag location that maximises signal-to-noise ratio (SNR) for both models. Numerical simulations validated the analytical claims and demonstrate that the specular model outperforms the diffuse model in SNR despite extra effort required for alignment, and the relationship between optimal tag location and the system parameters in the specular model is different compared to the one in the diffuse model.**

***Index Terms*—Visible light communication, backscatter communication, bi-static backscattering, optimisation**

I. Introduction

Backscatter communication has attracted substantial attention in the Internet of Things (IoT) and green communication field [1], [2]. Backscatter Visible light communication (VLC) offers advantages such as immunity to sniffing and radio-frequency (RF) interference, high transmission rate, power efficiency and battery-free [3], [4]. Bi-static topology [5] for backscatter communication shows higher scalability and lower device complexity [6]. Hence, there is a huge potential for a bi-static VLC backscatter system which possesses all the above advantages to be applied to various applications.

A. State-of-the-Art

VLC backscattering was first introduced in 2015 as RetroVLC [7]. RetroVLC proposed a practical design of a VLC backscatter tag with the nature of the retroreflector which always reflects the light along the incident direction and the liquid crystal display (LCD) shutter for signal modulation. In [4], the control of the LCD shutter was improved with a trend-based modulation scheme for better data rate and bandwidth utilisation. Recent studies also extend VLC backscattering with applications in the medical field [8] and in dynamic, drone-assisted environments [9].

On the other hand, there was research on backscatter architectures in RF communication systems. The differences between the conventional (mono-static) backscatter and bi-static backscatter systems were elaborated in [6] and [10]. It highlighted that the bi-static backscatter system has the advantages of a longer communication range, lower complexity and cost for the transmitter (Tx) and receiver (Rx). Also, bi-static backscatter topology enables tag-to-tag communication which could be used in a wider range of applications.

Prior studies were also carried out to enhance the performance of backscatter communication systems by optimising the location of nodes within the system. In [11], a study of the signal-to-noise ratio (SNR) performance between tags provided insight into optimising the location of the tag and transmitter in each travelled path within a large-scale system consisting of more than ten nodes. Moreover, the relationship between bit-error-rate (BER), SNR and communication distance was elaborated in [12] and [13].

B. Motivation and Contributions

We observe that the currently available designs of VLC backscattering architectures are based on the mono-static configuration introduced by RetroVLC [7]. The prior studies on bi-static configuration backscattering were limited to RF communication systems. To our best knowledge, the bi-static VLC backscatter system model, which can be very different from RF systems, has not been investigated much. A set of preliminary models for bi-static VLC backscatter systems was proposed in [14]. However, the proposed models have limitations on the tag alignment and are vague in the hardware designs. Moreover, the mathematical glitches in [14] lead to non-replicable conclusions. We would like to address this research gap with novel, achievable models that enable the practical construction of low-cost, high-throughput and long-range bi-static VLC backscatter systems for various applications in IoT.

Our four-fold contribution is summarized below.

- We propose two novel and practical bi-static VLC backscatter models based on the specular reflector and diffuse reflectors, respectively.
- We derive the closed-form expressions for the effective SNR of each model as a function of key system parameters such as distances among the Tx, Rx and tag.
- We present the global optimal tag location in each model to achieve the highest SNR.
- Numerical investigation is performed to validate the global optimality and to discourse the differences in the

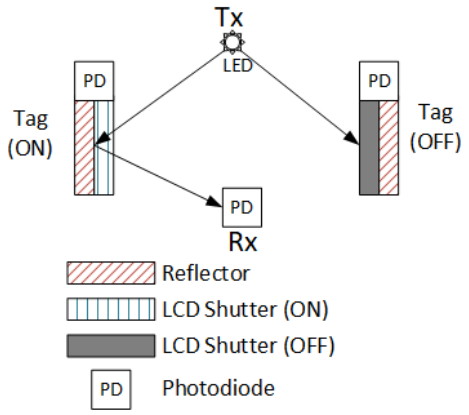

Fig. 1: Bi-static VLC backscatter topology.

optimal location between the two models under specific sets of system parameters.

II. System Description

We consider the VLC backscatter system comprising a light transmitter (Tx), a light receiver (Rx) and a backscatter tag. Light is emitted from the light-emitting diode (LED) source of Tx, and the photo-diode (PD) of Rx receives the light reflected (backscattered) from the tag. The design of the backscatter tag comprises a modulator, a reflector and a PD harvesting energy for tag operation as shown in Fig. 1 below. For the modulator, we adopt the liquid-crystal display (LCD) shutter design from Retro-VLC and its latter improvements [4], [7] which varies the light polarity with the power to the LCD panel and controls the passing/blocking with the two polariser films at each end, to achieve on-off keying (OOK) modulation. However, the retroreflector in the mono-static RetroVLC tag has to be replaced with other designs since Tx and Rx are located at different locations in the bi-static configuration. Thus, one of our goals is to design such a reflector. There are two possible options: a specular reflector such as a mirror, or a diffuse reflector that exhibits Lambertian reflection. To analyse the characteristics and the impact of reflector type on the performance of the tag, we evaluate both options by proposing a dedicated model for each.

SNR is one of the key metrics of overall performance quality in backscattering communication. The location of tags is a variable of interest that affects SNR. Thus, the other of our goals is to find optimal locations of tags to maximise SNR. SNR could be expressed as $\gamma_s = P_r/\sigma^2 = P_t h_s/\sigma^2$ where P_t, P_r, σ^2 and h_s represents the received power, transmitted power, noise variance and optical channel gain, respectively. In [15], assuming the field-of-view (FOV) of the receiver is 90°, the optical channel gain from a Lambertian emitter to a receiver surface was described as

$$h_s = \frac{(m+1)A_R}{2\pi R^2}\cos^m(\phi)\cos(\theta), \tag{1}$$

where A_R is the effective area of Rx, R denotes the distance between the light source and the point of incidence at Rx, m represents the Lambertian coefficient, ϕ denotes the emitting angle from the emitter, and θ denotes the incident angle at receiver.

III. Proposed Bi-static VLC Backscatter Models

A. Specular Model

The model based on the backscatter tag with a specular reflector is as illustrated in Fig. 2a below. The reflection from the specular reflector follows the law of reflection that the angle of reflection is always the same as the angle of incidence. Hence, it has the advantage of less power loss if the Rx is located in the direction of reflection since the reflected energy is concentrated in that direction. However, it also means that there will be huge energy loss due to poor alignment of Tx, tag and Rx. Thus, the downside of using a specular reflector is the extra effort required for light-of-sight (LoS) alignment. In particular to the configuration in Fig. 2a, the tilting angle β of the tag is $\beta = \frac{\theta-\phi}{2} = \frac{1}{2}(\arctan(\frac{s_r}{d}) - \arctan(\frac{s_t}{D-d}))$. In practical deployment, an alternative alignment method is possible with tools, for example, to use a laser pointer at Tx shining towards the tag, and manually adjusting the titling angle to align the reflected spot to the Rx.

We assume Tx and Rx are located on parallel planes and facing each other, with a fixed distance D, and the tag is tilted to the correct angle β to establish alignment of LoS. Assuming the specular reflector is a perfect mirror, the LoS propagation path from emission point O_t of Tx to incident point O_r of Rx via reflection point O of the tag is equivalent to an LoS path between the mirror image of emission point (denoted by O_t') and Rx incident point O_r, obstructed by a mirror with reflectivity ρ at point O [16]. As indicated in Fig. 2a, $\cos(\phi) = (D-d)/R_t$ and $\cos(\theta) = d/R_r$. Using Eq.(1) and with the assumption that the area of the tag and Rx is small compared to the distance between O_t' and O_r and Tx is a Lambertian emitter with $m = 1$, the channel power gain could be defined as

$$h_s = \frac{\frac{1}{\pi}A_R\rho d(D-d)}{\left(\sqrt{(D-d)^2+s_t^2}+\sqrt{d^2+s_r^2}\right)^2\sqrt{(D-d)^2+s_t^2}\sqrt{d^2+s_r^2}} \tag{2}$$

We assume the direct LoS from Tx to Rx is blocked, and there are no other reflectors in the system that introduce interference. For SNR, we apply the normalised distances that $\hat{d} = d/D$, $t = s_t/D$ and $r = s_r/D$. SNR for the specular model is calculated by

$$\gamma_s = \frac{\alpha_s\hat{d}(1-\hat{d})}{\left(\sqrt{(1-\hat{d})^2+t^2}+\sqrt{\hat{d}^2+r^2}\right)^2\sqrt{(1-\hat{d})^2+t^2}\sqrt{\hat{d}^2+r^2}}, \tag{3}$$

where $\alpha_s = \frac{P_t L_m \eta \rho A_R}{\pi\sigma^2 D^2}$, in which L_m is the efficiency of the LCD shutter and η is the photo-electronic conversion factor of Rx. α_s is independent of tag location.

B. Diffuse Model

The model based on the backscatter tag with a diffuse reflector is as illustrated in Fig. 2b below. In contrast to a

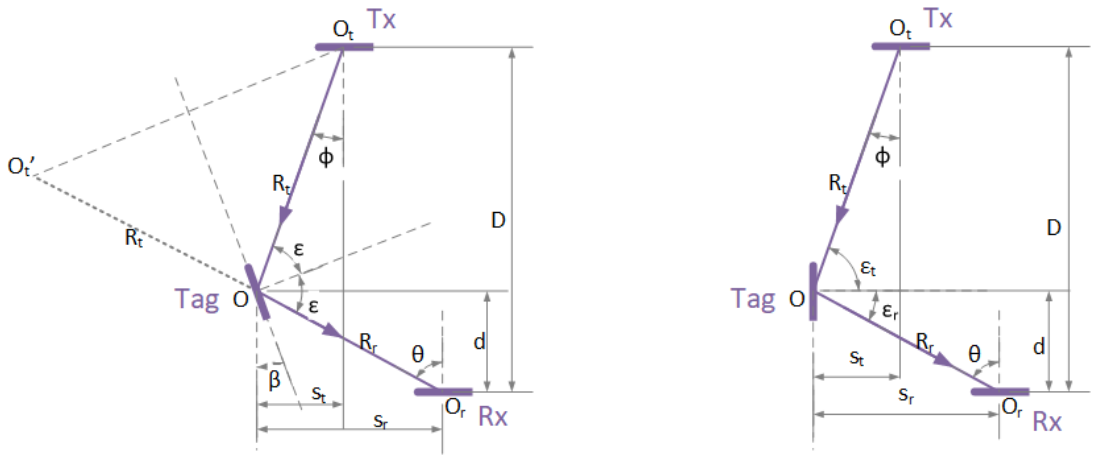

(a) Specular (b) Diffuse

Fig. 2: Bi-static backscatter model with (a) specular reflector; and (b) diffuse reflector.

specular reflector, a diffuse reflector requires no extra effort to compute the tilting based on the tag location since the incident light is scattered in different directions. However, it also means that the energy received by Rx is significantly lower than specular reflection since the reflected energy is distributed in different directions.

By using a diffuse reflector, it is equivalent to consider the reflector is another Lambertian emitter with $m = 1$, which has $P_t = \rho P_{incident}$. We assume the reflection plane of the diffuse reflector is perpendicular to Tx/Rx plane. Hence, the LoS propagation path O_t-O-O_r could be modeled as two LoS paths: one incident LoS path O_t-O, whose channel gain is denoted by h_{d1}; and a radiant LoS path whose channel gain is denoted by h_{d2} [16]. Note that the reflection angle ϵ_r can be different from the incident angle ϵ_t. Assume A_{tag} is the effective reflector area of the tag , the channel gain could be expressed as

$$h_{d1} = \frac{A_{tag}(D-d)s_t}{\pi((D-d)^2+s_t^2)^2}; \quad h_{d2} = \frac{A_R d s_r}{\pi(d^2+s_r^2)^2} \tag{4}$$

The corresponding signal-to-noise ratio (SNR), with normalised distances $\hat{d} = d/D$, $t = s_t/D$ and $r = s_r/D$, can be calculated by

$$\gamma_d = \alpha_d \cdot \frac{\hat{d}(1-\hat{d})tr}{((1-\hat{d})^2+t^2)^2(\hat{d}^2+r^2)^2}, \tag{5}$$

where $\alpha_d = \frac{P_t L_m \eta \rho A_{tag} A_R}{\pi^2 \sigma^2 D^4}$, which is independent of tag location.

Remark 1: It may be noted that the SNR expressions for the specular model and diffuse model are different, which implies that to enhance their performance, we need to investigate them separately.

IV. Optimal Tag Location

A. Optimisation Problem Formulation

As stated in Section II, one of our goals is to find the optimal tag location to maximise SNR. We assume D, s_t and s_r are predetermined key system parameters. The optimal tag location in terms of vertical distance to Rx could be represented as the optimisation problems as shown below.

The corresponding optimisation problem (P1) for the specular model is given as

$$\begin{aligned} (P1): \ &\max_{\hat{d}} \ \gamma_s, \\ &s.t. \ \ C1: \ \hat{d} \le 1-\delta, \ \ C2: \ \hat{d} \ge \delta. \end{aligned} \tag{6}$$

The constraint $C1$ and $C2$ are to ensure the tag is located in the far-field region, where $\delta = \delta_0/D$ and δ_0 is the minimum distance required for far-field condition [17]. The corresponding optimisation problem (P2) for the diffuse model is given by

$$(P2): \ \max_{\hat{d}} \ \gamma_d, \qquad s.t. \qquad C1, C2. \tag{7}$$

It can be noted that the constraints in optimisation problems (P1) and (P2) are the same. However, as observed from the SNR formula as Eq.(3) and Eq.(5), the SNR are very different from the two models.

We discuss the global optimal solution to each model in the next section.

B. Global Optimal Solution

1) Convexity analysis: First, it can be noted that both optimisation problem (P1) and (P2) are not convex because the underline objective functions γ_s and γ_d are not concave in their respective feasible region as defined by $C1$ and $C2$. This will result in multiple maxima and minima, that is, multiple local optimal solutions. However, the constraint $C1$ and $C2$ are linear and boxed constraints. Thus, to find the global solution to the problem, we have to find all the local solutions.

2) Optimal solution for specular model: The local optimisers to the optimisation problems are the stationary points found by setting the first derivatives of the objective function equal

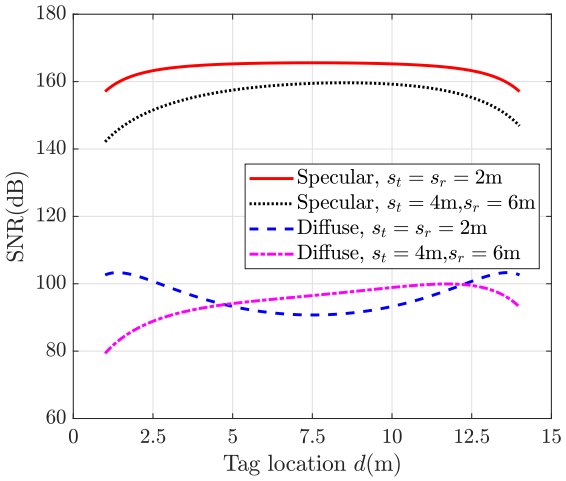

Fig. 3: SNR performance of models under system parameter sets $s_t = s_r = 2$m and $s_t = 4$m, $s_r = 6$m.

to zero. After simplification, we get a 10-order polynomial equation in $\hat{d}$ as given below for problem (P1).

$$\begin{aligned}
&4\hat{d}^2r^6t^4 - 4\hat{d}r^6t^4 + 4\hat{d}^4r^6t^2 - 14\hat{d}^3r^6t^2 + 18\hat{d}^2r^6t^2 \\
&- 10\hat{d}r^6t^2 + \hat{d}^6r^6 - 6\hat{d}^5r^6 + 15\hat{d}^4r^6 - 20\hat{d}^3r^6 + 15\hat{d}^2r^6 \\
&- 6\hat{d}r^6 - 4\hat{d}^2r^4t^6 + 4\hat{d}r^4t^6 + 12\hat{d}^3r^4t^4 - 18\hat{d}^2r^4t^4 \\
&+ 12\hat{d}r^4t^4 - 3\hat{d}^6r^4t^2 + 12\hat{d}^5r^4t^2 - 21\hat{d}^4r^4t^2 + 24\hat{d}^3r^4t^2 \\
&- 21\hat{d}^2r^4t^2 + 12\hat{d}r^4t^2 - 4\hat{d}^8r^4 + 22\hat{d}^7r^4 - 49\hat{d}^6r^4 \\
&+ 56\hat{d}^5r^4 - 35\hat{d}^4r^4 + 14\hat{d}^3r^4 - 7\hat{d}^2r^4 + 4\hat{d}r^4 - 4\hat{d}^4r^2t^6 \\
&+ 2\hat{d}^3r^2t^6 + 3\hat{d}^6r^2t^4 - 6\hat{d}^5r^2t^4 + 6\hat{d}^4r^2t^4 - 12\hat{d}^7r^2t^2 \\
&+ 42\hat{d}^6r^2t^2 - 54\hat{d}^5r^2t^2 + 30\hat{d}^4r^2t^2 - 6\hat{d}^3r^2t^2 - 4\hat{d}^{10}r^2 \\
&+ 20\hat{d}^9r^2 - 36\hat{d}^8r^2 + 20\hat{d}^7r^2 + 20\hat{d}^6r^2 - 36\hat{d}^5r^2 + 20\hat{d}^4r^2 \\
&- 4\hat{d}^3r^2 - \hat{d}^6t^6 + 4\hat{d}^8t^4 - 10\hat{d}^7t^4 + 7\hat{d}^6t^4 + 4\hat{d}^{10}t^2 \\
&- 20\hat{d}^9t^2 + 36\hat{d}^8t^2 - 28\hat{d}^7t^2 + 8\hat{d}^6t^2 + r^6t^4 \\
&+ 2r^6t^2 + r^6 - r^4t^6 - 3r^4t^4 - 3r^4t^2 - r^4 = 0.
\end{aligned} \tag{8}$$

With any given system parameter of t and s, we could find all 10 roots of the above polynomial equation numerically. These 10 roots are functions of t and s. We collect the real roots that satisfy the constraint $C1$ and $C2$ and store them in a vector $\mathbf{d}_s$ along with the boundary points, δ and $1-\delta$, where the i^{th} root is denoted by $[\mathbf{d}_s]_i$. Assume there are k_s real roots satisfying the constraints ($k_s \leq 10$), then the length of the vector will be $k_s + 2$. Thus, the global solution is

$$d_s^* = \underset{1\leq i\leq k_s+2}{\operatorname{argmax}} \ \gamma_s\left([\mathbf{d}_s]_i\right). \tag{9}$$

3) Optimal solution for diffuse model: Similar to (P1), when we take the first derivative of the objective function γ_d with respect to $\hat{d}$ for (P2), we get a 5-order polynomial equation as given below.

$$\begin{aligned}
&-2\hat{d}r^2t^2 + 2\hat{d}^3r^2 - 3\hat{d}^2r^2 + 2\hat{d}^3t^2 - 3\hat{d}^2t^2 + 6\hat{d}^5 \\
&- 15\hat{d}^4 + 12\hat{d}^3 - 3\hat{d}^2 + r^2t^2 + r^2 = 0.
\end{aligned} \tag{10}$$

Again, we could find all 5 roots of the above polynomial equation numerically with any given system parameter of t and s. We collect the real roots that satisfy the constraint $C1$ and $C2$ and store them in a vector $\mathbf{d}_d$ along with the boundary points, δ and $1-\delta$, where the i^{th} root is denoted by $[\mathbf{d}_d]_i$. Assume there are k_d real roots satisfying the constraints ($k_d \leq 5$), then the length of the vector will be $k_d + 2$. Thus, the global solution for (P2) could be expressed as

$$d_d^* = \underset{1\leq i\leq k_d+2}{\operatorname{argmax}} \ \gamma_d\left([\mathbf{d}_d]_i\right). \tag{11}$$

Thus we conclude that we have obtained the global optimal solutions for both (P1) and (P2). We can easily obtain the roots of polynomial functions using in-built functions in commercial software like Matlab. In the next section, we will verify the non-convexity of (P1) and (P2) along with insights on the optimal location, which can provide significant gains over the non-optimal conventional locations.

V. Numerical Results

Unless explicitly stated, we have used $D = 15$m, $A_{tag} = A_R = 0.4\text{m}^2$, $P_t = 10$W, $L_m = 0.5$, $\eta = 0.7$, $\sigma^2 = -70$dBm, $\delta_0 = 1$m, and $\rho = 0.9$ for both models.

Firstly, to understand the performance of the models, we evaluate the SNR (in dB) comparison between the specular model and diffuse model under different sets of system parameters (s_t and s_r), as shown in Fig.3. The results validated that the SNR expressions are non-concave, especially for the diffuse model, which results in multiple maxima and minima. It is also observable that although the models behave differently in terms of SNR over the tag location, SNR for the diffuse model is much lower than the one for the specular model with every tag location, which validates the statement in Section III-B. Moreover, with reference to the SNR at optimal location, the percentage loss of SNR when tag at location of minimum SNR are 5.15% and 10.97% for specular model and 12.17% and 20.61% for diffuse model, in the scenario of $s_t = s_r = 2$m and $s_t = 4$m, $s_r = 6$m respectively. This highlights the necessity of optimisation of the tag location. Secondly, we evaluate the relationship between the optimal tag location d and the system parameters s_t and s_r. We present the variation of optimal d with the change of s_r in four scenarios where s_t sets to 2m, 4m, 6m and 8m respectively. Different relationships in the specular model and diffuse model are illustrated in Fig.4a and Fig.4b respectively. We could observe the following:

1) When Tx and Rx are vertically aligned, that is, when $s_t = s_r$, the optimal location is always at the centre ($d = 0.5D$) for specular model; In contrast, diffuse model has two different behaviour depending on the actual value of s_t and s_r. When $s_t = s_r = 2$m or $s_t = s_r = 4$m , there are two optimal locations close Tx and Rx. The centre point is the optimal location when $s_t = s_r = 6$m or $s_t = s_r = 8$m.
2) When Tx and Rx are vertically misaligned, that is, when $s_t \neq s_r$, the optimal location shifts from the one under

aligned condition towards the node (Tx or Rx) with a shorter horizontal distance. Assume the optimal location for Tx/Rx aligned is at d_0, if distance to Tx is shorter ($s_t < s_r$), the optimal location will be closer to Tx ($d > d_0$), and vice-versa.

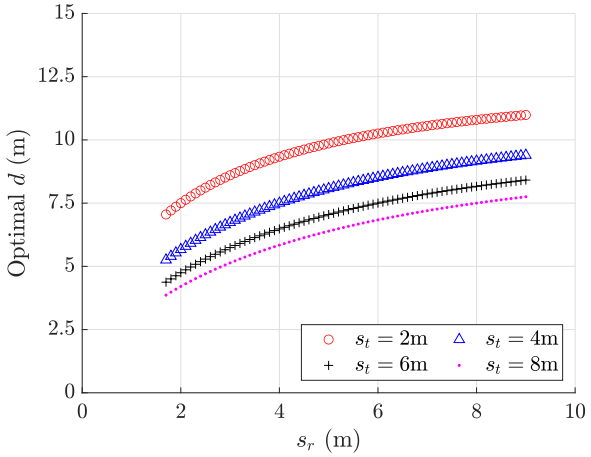

(a) Specular model

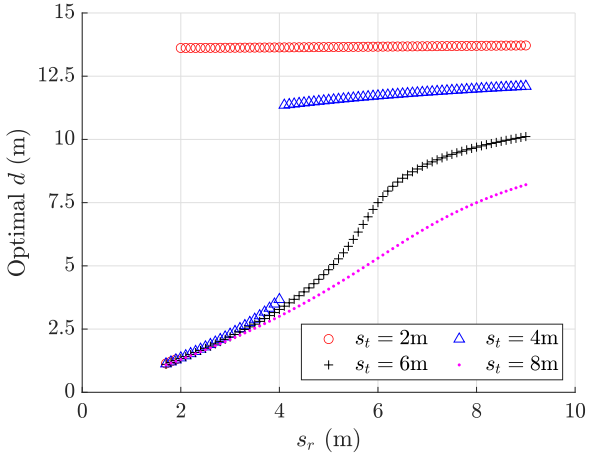

(b) Diffuse Model

Fig. 4: Optimal tag location under different system parameter sets for (a) specular model and (b) diffuse model.

VI. Conclusion

Bi-static VLC backscatter system has potential advantages like low-cost, high throughput and long range. This work proposed two novel bi-static VLC backscatter models with the specular reflector and diffuse reflector, respectively. Also, this work investigated the optimal tag location for maximum SNR in each model. We elaborated the configuration, channel model and SNR expression for each proposed model, and showed that the optimal vertical locations of the tag could be derived from roots of polynomial equations once the system parameters are determined. The numerical investigation validated that the specular model has better SNR performance than the diffuse model despite the extra effort needed for alignment, and showed the relationship between the optimal tag locations and the variation of system parameters. In future, we would like to extend these models to tag-to-tag communication topology. Also, we would like to study the behaviour of the model under interference, such as reflections from walls near the tag.

VII. Acknowledgment

This research work has been supported in part by the Australian Research Council Discovery Early Career Researcher Award (DECRA) - DE230101391.

References

[1] J.-P. Niu and G. Y. Li, "An overview on backscatter communications," *Journal of Communications and Information Networks*, vol. 4, no. 2, pp. 1–14, 2019.

[2] D. Mishra and E. G. Larsson, "Multi-tag backscattering to MIMO reader: Channel estimation and throughput fairness," *IEEE Transactions on Wireless Communications*, vol. 18, no. 12, pp. 5584–5599, 2019.

[3] S.-H. Lin, C. Liu, X. Bao, and J.-Y. Wang, "Indoor visible light communications: performance evaluation and optimization," *EURASIP Journal on Wireless Communications and Networking*, vol. 2018, no. 1, p. 228, 2018.

[4] X. Xu, Y. Shen, J. Yang, C. Xu, G. Shen, G. Chen, and Y. Ni, "PassiveVLC: Enabling practical visible light backscatter communication for battery-free IoT applications," in *Proc. ACM MobiCom*, Snowbird, Utah, USA, Oct 2017, p. 180–192.

[5] L. Qu, D. Mishra, and J. Yuan, "Channel estimation protocol for bistatic backscattering using multiantenna transceiver," in *Proc. IEEE PIMRC*, 2022, pp. 439–444.

[6] N. Van Huynh, D. T. Hoang, X. Lu, D. Niyato, P. Wang, and D. I. Kim, "Ambient backscatter communications: A contemporary survey," *IEEE Communications Surveys & Tutorials*, vol. 20, no. 4, pp. 2889–2922, 2018.

[7] J. Li, A. Liu, G. Shen, L. Li, C. Sun, and F. Zhao, "Retro-VLC: Enabling battery-free duplex visible light communication for mobile and IoT applications," in *Proc ACM HotMobile*, Santa Fe, New Mexico, USA, Feb 2015, p. 21–26.

[8] M. H. Ullah, G. Gelli, and F. Verde, "Visible light backscattering communications in healthcare scenarios: link modeling and performance analysis," in *Proc. IEEE IoTaIS*, Bali, Indonesia, Nov 2022, pp. 179–185.

[9] L. De Groot, T. Xu, and M. Z. Zamalloa, "DroneVLC: Exploiting drones and VLC to gather data from batteryless sensors," in *Proc. IEEE PerCom*, Atlanta, USA, Mar 2023, pp. 242–251.

[10] P. Wilmoth, T. Wardak, Y. Ineza, S. Givens, C. Peroni, G. Sklivanitis, and D. Pados, "Demo: Bi-static scatter underwater acoustic communications," in *Proc. ACM WUWNet*, Boston, MA, USA, Nov 2022.

[11] X. Wang, K. Han, and M. Zhang, "Modeling the large-scale visible light backscatter communication network," in *Proc. APCC*, Perth, Australia, Dec 2017, pp. 1–6.

[12] S. Shao, A. Khreishah, and H. Elgala, "Pixelated VLC-backscattering for self-charging indoor IoT devices," *IEEE Photonics Technology Letters*, vol. 29, no. 2, pp. 177–180, 2017.

[13] S. M. Navidpour, M. Uysal, and M. Kavehrad, "BER performance of free-space optical transmission with spatial diversity," *IEEE Transactions on Wireless Communications*, vol. 6, no. 8, pp. 2813–2819, 2007.

[14] W. Lin and D. Mishra, "Enhancement of visible light backscatter communication by optimally locating the tags," in *Proc. EUSIPCO*, Dublin, Ireland, Aug 2021, pp. 1606–1610.

[15] T. Komine and M. Nakagawa, "Fundamental analysis for visible-light communication system using LED lights," *IEEE Transactions on Consumer Electronics*, vol. 50, no. 1, pp. 100–107, 2004.

[16] Y. Wu, P. Audenaert, M. Pickavet, and D. Colle, "Mirror-aided non-LOS VLC channel characterizations with a time-efficient simulation model," *Photonic Network Communications*, vol. 38, no. 1, p. 151–166, Aug 2019.

[17] I. Moreno, C.-C. Sun, and R. Ivanov, "Far-field condition for light-emitting diode arrays," *Applied Optics*, vol. 48, no. 6, pp. 1190–1197, Feb 2009.